Journal of Power Sources 210 (2012) 321–326

Contents lists available at SciVerse ScienceDirect

Journal of Power Sources

journal homepage: www.elsevier.com/locate/jpowsour

Short communication

Preparation of $Pt/Ir_x(IrO_2)_{10-x}$ bifunctional oxygen catalyst for unitized regenerative fuel cell

Fan-Dong Kong[a,b], Sheng Zhang[a], Ge-Ping Yin[a,*], Na Zhang[a], Zhen-Bo Wang[a], Chun-Yu Du[a]

[a] School of Chemical Engineering and Technology, Harbin Institute of Technology, 150001 Harbin, China
[b] School of Physical Sciences, Ji-ning Medical University, 272000 Ji-ning, China

ARTICLE INFO

Article history:
Received 17 November 2011
Received in revised form 4 February 2012
Accepted 6 February 2012
Available online 26 March 2012

Keywords:
Platinum–iridium catalyst
Bifunctional oxygen catalyst
Unitized regenerative fuel cell

ABSTRACT

Bifunctional $Pt/Ir_x(IrO_2)_{10-x}$ ($x < 10$) catalyst for unitized regenerative fuel cell (URFC) has been prepared by depositing Pt on $Ir_x(IrO_2)_{10-x}$ support which is obtained initially from Adams fusion method. X-ray diffraction and transmission electron microscopy show that ultrafine and narrow distributed $Pt/Ir_3(IrO_2)_7$ nanocomposites are formed. Electrochemical measurements demonstrate that among the series of catalysts studied, $Pt/Ir_3(IrO_2)_7$ catalyst possesses the highest electrochemical surface area ($24.74\,m^2\,g^{-1}$) and the highest activity towards oxygen reduction reaction (ORR) ($21.71\,mA\,mg^{-1}$ at 0.85 V). Meanwhile, considerably high activity towards oxygen evolution reaction (OER) ($42.35\,mA\,mg^{-1}$ at 1.55 V) is also observed for $Pt/Ir_3(IrO_2)_7$ catalyst. Kinetic analyses indicate that ORR on $Pt/Ir_3(IrO_2)_7$ catalyst follows four-electron mechanism. This work opens a new way to fabricate efficient bifunctional oxygen catalyst for URFC.

1. Introduction

A unitized regenerative fuel cell (URFC), analogous to rechargeable battery, is an energy conversion and storage device using hydrogen as an energy carrier. It works both as H_2/O_2 fuel cell and as water electrolyser with a single operation unit [1,2]. The theoretical energy density of URFC reaches as high as $3600\,Wh\,kg^{-1}$. Although it would be reduced to 400–$1000\,Wh\,kg^{-1}$ when the mass of tanks of H_2, O_2, and water, as well as the mass of URFC itself are taken into account, the energy density is still several times higher than that of any batteries [3–6]. The applications of URFC is associated with relatively large amount of energy storage, including remote off-grid power sources, emergency or back-up power generation, zero emission vehicles, hybrid energy storage/propulsion systems for space aircraft, and high altitude long endurance solar rechargeable aircraft [7–10].

In URFC design, Pt nanoparticles serving as bifunctional hydrogen catalyst (BHC) has attained excellent performance, but bifunctional oxygen catalyst (BOC) has still remained a problem concerning irreversible oxygen redox reaction [11]. The preferred oxygen reduction reaction (ORR) catalysts demonstrate poor oxygen evolution reaction (OER) performance, and the preferred OER catalysts demonstrate poor ORR performance [12]. Currently, Pt/IrO_2 nanocomposite is commonly considered an excellent BOC [13–15], in which Pt functions as ORR catalyst [16–19], while IrO_2 as OER catalyst [20–22]. However, Pt/IrO_2 catalysts prepared by previous methods can easily agglomerate, resulting in poor interdispersion of the two kinds of catalysts and low bifunctional catalytic performance [23]. On the other hand, IrO_2 agglomerates with higher ohmic resistance trend to block the electronic paths between Pt particles, leading to Pt insufficient performance [15,24]. Therefore, exploring an effective route to prepare Pt/IrO_2 nanocomposite with uniform distribution and high electronic conductivity is of significance for BOC fabrication and URFC development [25].

In this study, we detailedly investigated $Pt/Ir_x(IrO_2)_{10-x}$ ($x < 10$) catalyst with varying Ir and IrO_2 ratio. $Ir_x(IrO_2)_{10-x}$ support, serving as OER catalysts as well, was prepared initially from Adams fusion method. It is expected that the optimization between Ir and IrO_2 contents could improve the conductivity of the support and achieve overall enhancement of catalytic performance. To the best of our knowledge, this work was first accomplished in our group aiming at exploring a new route to fabricate efficient BOCs for URFC.

2. Experimental

2.1. Preparation of catalysts

Adams' method has successfully been used for preparation of anode catalysts such as platinum oxide, iridium oxide, and ruthenium oxide by several groups [1,26,27]. It is proved a fast and convenient way to prepare those oxides with high specific surface

* Corresponding author at: School of Chemical Engineering and Technology, Harbin Institute of Technology, No. 92, West Da-Zhi Street, Harbin 150001, China. Tel.: +86 451 86413707; fax: +86 451 86413707.
E-mail address: yingeping@hit.edu.cn (G.-P. Yin).

0378-7753/$ – see front matter © 2012 Elsevier B.V. All rights reserved.
doi:10.1016/j.jpowsour.2012.02.021

area. For preparation of IrO_2 nanoparticles, 172 mg metal precursor ($IrCl_3 n{\cdot}H_2O$, Sino-Platinum Metals Co.) were dissolved in distilled water. Then, 50 g of $NaNO_3$ was added and stirred to uniformity. The mixture was carefully evaporated to dryness at 70 °C. The dried mixture was introduced into a ceramic furnace, heated to 350 °C at 10 °C min^{-1} (keeping for 15 min) and further heated to 450 °C at 5 °C min^{-1} (keeping for 30 min). After cooling to room temperature, the mixture was washed, filtered and dried in a vacuum oven at 80 °C.

For preparation of $Ir_x(IrO_2)_{10-x}$ composites, Ir was deposited on the surface of IrO_2 nanoparticles through microwave-assisted polyol process (MAPP) [28]. The molar ratios of Ir to IrO_2 were 0:10, 1:9, 2:8, 3:7, and 4:6. Briefly, desired amount of $IrCl_3{\cdot}nH_2O$ was dissolved in a solution containing glycol and isopropanol. Then, desired amount of IrO_2 was added. After ultrasonic treatment for 30 min, the solution was adjusted to a pH value of 12 and stirred for 2 h, followed by heating in microwave oven for 50 s (ca. 130 °C). After cooling to room temperature, the solution was adjusted with 0.5 M HNO_3 to a pH value within 3–4 and continuously stirred for 10 h. Subsequently, the resulting mixture was centrifuged and rinsed repeatedly until no Cl^- ions in the residue solution were detected, then dried in a vacuum oven at 80 °C.

The preparation of $Pt/Ir_x(IrO_2)_{10-x}$ catalyst was conducted by deposition of Pt onto $Ir_x(IrO_2)_{10-x}$ support. Similar MAPP method described above was also employed, in which the metal precursor, H_2PtCl_6, (Sino-Platinum Metals Co.) was used instead of $IrCl_3{\cdot}nH_2O$. The nominal concentrations in $Pt/Ir_x(IrO_2)_{10-x}$ catalyst were 50 mol% Pt and 50 mol% Ir (Ir element content).

2.2. Materials characterization

The X-ray diffraction (XRD) patterns of the catalysts were recorded using a D/max-rB X-ray diffractometer (Japan). Cu Kα was used as radiation source operating at 45 kV and 100 mA. The samples were tested in the angle (2θ) range from 10° to 90° at 4° min^{-1} with an resolution of 0.05°.

Transmission electron microscopy (TEM) images of the catalysts were taken using a JEOL TEM-1200EX (Netherlands) system with a spatial resolution of 1 nm. The samples were finely ground and ultrasonically dispersed in ethanol, and a drop of the resultant dispersion was covered and dried on a standard carbon membrane substrates. The operating voltage on the microscope was 120 keV for low-resolution tests and 300 keV for high-resolution tests.

2.3. Electrochemical measurements

For the preparation of working electrode, glassy carbon rotating disc electrode (GC RDE) of 3 mm in diameter (0.07065 cm^2) was polished with 0.05 μm alumina to a mirror-finish before each experiment. The ink with the total metals concentration of 2 mg ml^{-1} was prepared by ultrasonically dispersing catalysts in ethanol/water (1:1 by volume). Four microliters of the ink was loaded on GC RDE and dried in argon atmosphere. That operation was repeated another two time. After completely drying, it was covered with 4 μl of dilute Nafion solution (5 wt.%, DuPont Co. Ltd.) to form a thin protective film [29,30].

The electrochemical measurements were conducted with GC RDE in a three-electrode electrochemical cell. GC RDE covered with catalysts serves as the working electrode, Pt foil of 1 cm^2 as the counter electrode and Hg/Hg_2SO_4 electrode as the reference electrode. Experiments were performed in 0.5 M H_2SO_4 solution at 25 °C using CHI650C electrochemical analysis instrument (Shanghai, China). Before recording, the catalysts were activated through cyclic voltammetry (CV) scanning in the range of 0.05–1.2 V at a scan rate of 50 mV s^{-1} until steady CV curves were obtained. To determine the electrochemical surface area (ESA), the CVs were recorded in an argon-purged 0.5 M H_2SO_4 solution in the range of 0.05–1.2 V at 20 mV s^{-1}. To evaluate the polarization of OER, the linear sweep voltammograms (LSVs) were recorded in the range of 1.2–1.65 V at 5 mV s^{-1}. Similarly, the LSVs for ORR were also recorded on GC RDE with a series of rotation speeds within the potential range of 1.1–0.4 V at 5 mV s^{-1} in an oxygen-saturated 0.5 M H_2SO_4 solution [31–33]. The electrochemical impedance spectra (EIS) were recorded at 1.55 V (OER) and 0.85 V (ORR) in the frequency range of 10,000–0.01 Hz with an amplitude of the sinusoidal potential perturbation of 5 mV.

In this study, chemicals applied were of analytical grade and the solutions were prepared with ultrapure water (MilliQ Millipore, 18.2 MΩ cm). All the potentials are with respect to standard hydrogen electrode (SHE).

3. Results and discussion

3.1. Characterization of $Pt/Ir_x(IrO_2)_{10-x}$ catalysts

Fig. 1 shows the XRD patterns of the synthesized $Pt/Ir_x(IrO_2)_{10-x}$ catalysts. And the main peaks of IrO_2 (JCPDS: 65-2822), Ir (JCPDS: 65-1686), and Pt (JCPDS: 65-2868) are indicated in the bottom of Fig. 1. From Fig. 1a, the diffraction peaks of IrO_2 and Pt with a feature of broadening indicate the presence of ultrafine nanoparticles. Similar feature is also found for the other catalysts. From Fig. 1b–e, the spectra exhibit almost the same profiles since Pt, Ir, and IrO_2 coexist in all the samples. The peak intensity of IrO_2 reduces gradually, whereas that of Pt or Ir (adjacent) increases with the increase of Ir content from a to e. However, it should be noted that the peak positions of Pt and Ir are so close that we cannot identify them. In other words, each diffraction peak observed is the overlap of the Pt peak with the Ir peak. Since Pt content (50 mol%) is identical in all the catalysts, the increase in peak intensity is mainly resulted from the increased Ir content. Another possible case to increase the peak intensity is that the depositing Pt atoms grow on Ir lattices to form larger duplex grains because crystallite Pt and Ir have similar lattices.

Fig. 2a and b shows the TEM images of $Pt/Ir_2(IrO_2)_8$ and $Pt/Ir_3(IrO_2)_7$ catalysts with high resolution. It can be seen that there is no substantial difference between the two catalysts in morphology. The particles are dispersed uniformly and the clear crystalline texture is an indication of Ir, Pt nanoparticles deposited on IrO_2 support. Fig. 2c and e displays the wide-scope observations for

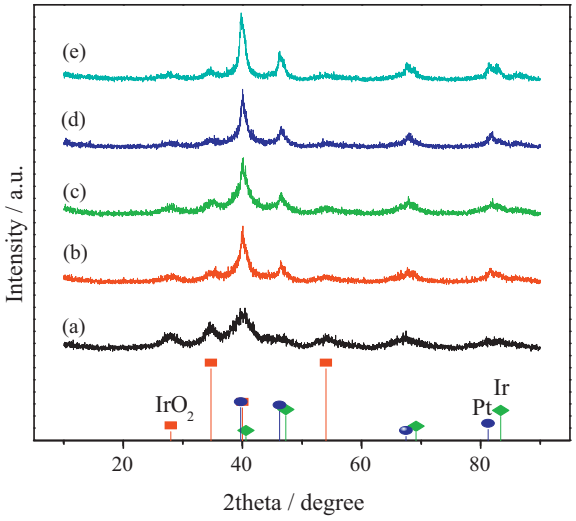

Fig. 1. XRD patterns of the catalysts, $Pt/Ir_0(IrO_2)_{10}$ (a), $Pt/Ir_1(IrO_2)_9$ (b), $Pt/Ir_2(IrO_2)_8$ (c), $Pt/Ir_3(IrO_2)_7$ (d), $Pt/Ir_4(IrO_2)_6$ (e).

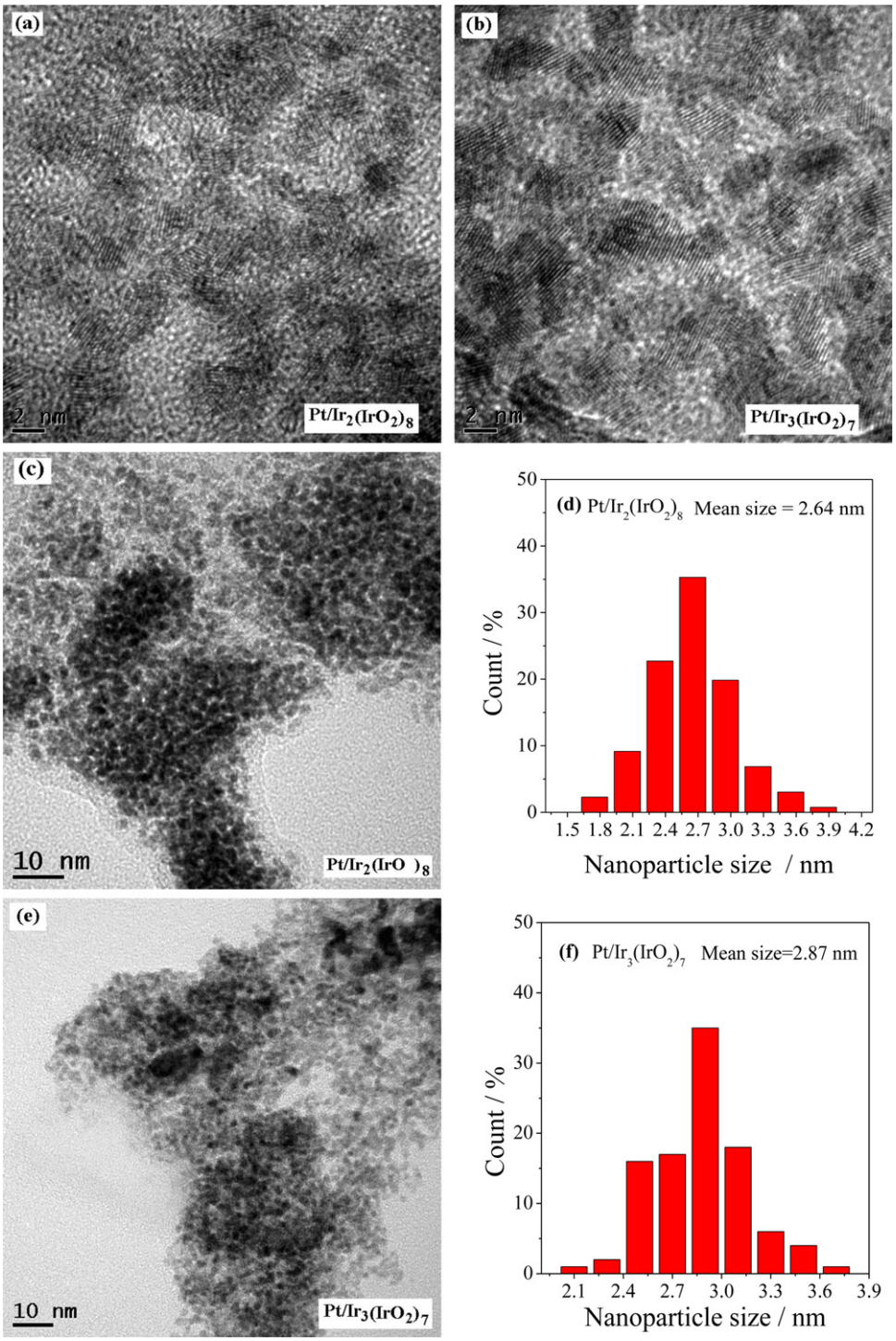

Fig. 2. TEM images of $Pt/Ir_2(IrO_2)_8$ (a and c) and $Pt/Ir_3(IrO_2)_7$ (b and e) catalysts, and their particle size distributions (d and f).

$Pt/Ir_2(IrO_2)_8$ and $Pt/Ir_3(IrO_2)_7$ catalysts, and in each figure narrow distribution of the nanocomposites is clearly found. The particle size distributions of $Pt/Ir_2(IrO_2)_8$ and $Pt/Ir_3(IrO_2)_7$ nanocomposites is shown in Fig. 2d and f, and their mean diameters are estimated to be 2.64 and 2.87 nm.

3.2. Cyclic voltammetry

Fig. 3 shows the cyclic voltammograms of $Pt/Ir_0(IrO_2)_{10}$, $Pt/Ir_1(IrO_2)_9$, $Pt/Ir_2(IrO_2)_8$, $Pt/Ir_3(IrO_2)_7$, $Pt/Ir_4(IrO_2)_6$ catalysts in 0.5 M H_2SO_4. Typical hydrogen and oxygen adsorption/desorption behaviors can be distinctly observed on the catalysts (a–e). Since Ir and IrO_2 have negligible contribution to the electrochemical surface areas (ESAs) (dot lines), the ESAs of $Pt/Ir_0(IrO_2)_{10}$, $Pt/Ir_1(IrO_2)_9$, $Pt/Ir_2(IrO_2)_8$, $Pt/Ir_3(IrO_2)_7$, $Pt/Ir_4(IrO_2)_6$ catalysts are calculated to be 17.02, 17.51, 23.07, 24.74, and 19.87 $m^2\ g^{-1}$, respectively [34]. This result indicates that $Pt/Ir_3(IrO_2)_7$ possesses the largest electrochemical surface area among these catalysts. The presence of Ir nanoparticles can improve the electronic conductivity of Pt/IrO_2 nanocomposite. And the role of IrO_2 nanoparticles in the nanocomposite is to enhance the dispersion of Pt, which will improve the Pt utilization. Since the total mass of Ir elements are kept unchanged

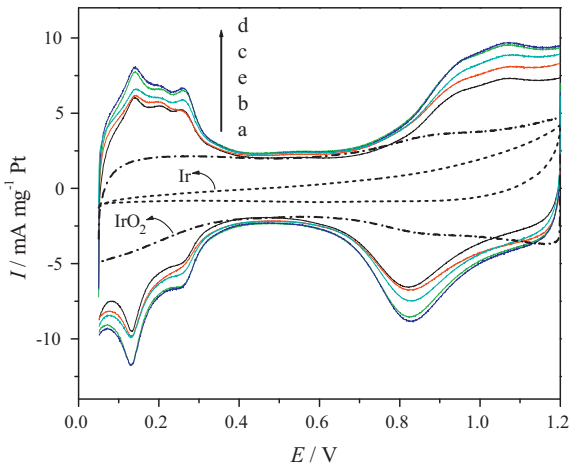

Fig. 3. Cyclic voltammograms of the catalysts, $Pt/Ir_0(IrO_2)_{10}$ (a), $Pt/Ir_1(IrO_2)_9$ (b), $Pt/Ir_2(IrO_2)_8$ (c), $Pt/Ir_3(IrO_2)_7$ (d), $Pt/Ir_4(IrO_2)_6$ (e), and pure Ir, IrO_2 (dot lines).

in our study, there exists an optimal ratio of Ir to IrO_2, which make the Pt, Ir, IrO_2 nanocomposite achieve the highest electrochemical surface area. Therefore, appropriate ratio of Ir to IrO_2 is 3:7, which obtains the highest ESA.

3.3. Oxygen reduction activity of $Pt/Ir_x(IrO_2)_{10-x}$ catalysts

The ORR activities on the catalysts are investigated using linear sweep voltammograms (Fig. 4a) and electrochemical impedance spectra (Fig. 4b). In Fig. 4a, all the catalysts show two different regions: one region with mixed kinetic diffusion control (0.7–0.9 V), and the other region with mass transfer control (<0.7 V). The oxygen-reduction kinetic currents can be obtained with the well-known mass-transport correction for rotating disk electrodes [34]:

$$I_k = \frac{I_d \times I}{I_d - I} \quad (1)$$

where I_k is the mass-transfer-free kinetically controlled ORR current, I_d is the measured diffusion-limited current, and I is the experimentally obtained current (with background subtraction). And the kinetic currents (I_k) for $Pt/Ir_0(IrO_2)_{10}$, $Pt/Ir_1(IrO_2)_9$, $Pt/Ir_2(IrO_2)_8$, $Pt/Ir_3(IrO_2)_7$, and $Pt/Ir_4(IrO_2)_6$ catalysts measured at 0.85 V are calculated to be 8.87, 9.17, 16.9, 21.71, and 14.88 mA mg^{-1}, respectively, which is consistent with the results of Pt ESA above.

Electrochemical impedance spectra recorded at 0.85 V are shown in Fig. 4b. The arc diameter is a measure of polarization resistance (Rct). It is clearly seen that the Rct value of the catalyst reduces in the order of $Pt/Ir_0(IrO_2)_{10} > Pt/Ir_1(IrO_2)_9 > Pt/Ir_4(IrO_2)_6 > Pt/Ir_2(IrO_2)_8 > Pt/Ir_3(IrO_2)_7$, indicating the increasing order in ORR activity. This result is in good agreement with that from LSV analysis.

3.4. Oxygen evolution activity of $Pt/Ir_x(IrO_2)_{10-x}$ catalysts

Fig. 5 shows the OER activities of the catalysts as a function of the mole ratio between Ir and IrO_2. From Fig. 5a, the current densities for $Pt/Ir_0(IrO_2)_{10}$, $Pt/Ir_1(IrO_2)_9$, $Pt/Ir_2(IrO_2)_8$, $Pt/Ir_3(IrO_2)_7$, and $Pt/Ir_4(IrO_2)_6$ catalysts measured at 1.55 V are 18.8, 31.24, 45.69, 42.35, and 31.68 mA mg^{-1}, respectively. This result reveals that the OER activity increases with Ir content up to 2:8 (mole ratio, Ir:IrO_2) followed by a activity decrease with further higher Ir content. In other words, $Pt/Ir_2(IrO_2)_8$ catalyst has the highest OER activity. Meanwhile, quite close OER activity for $Pt/Ir_3(IrO_2)_7$ catalyst is also observed. Fig. 5b shows the electrochemical

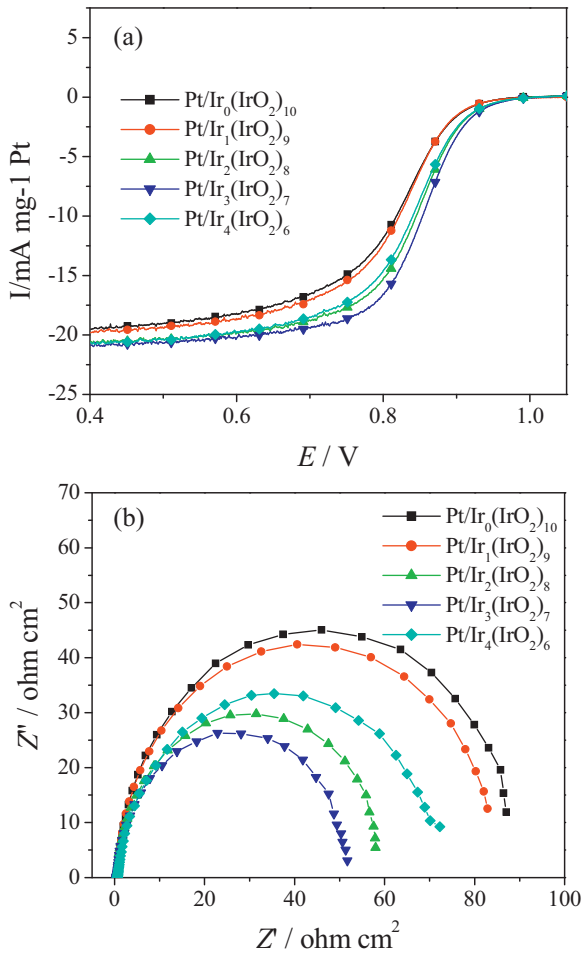

Fig. 4. Oxygen reduction activity measured with LSV (a) and EIS (0.85 V) (b) as a function of various compositions of $Pt/Ir_x(IrO_2)_{10-x}$ catalysts.

impedance spectra of the catalysts recorded at 1.55 V. From the arc diameters of the curves we attain Rct values in the order of $Pt/Ir_0(IrO_2)_{10} > Pt/Ir_1(IrO_2)_9 > Pt/Ir_4(IrO_2)_6 > Pt/Ir_3(IrO_2)_7 > Pt/Ir_2(IrO_2)_8$. This result is consistent with that from Fig. 5a.

The order of OER activity, however, is not matched with that of ORR activity. The reason for this is that the ORR activity is determined by Pt catalyst. Higher Pt dispersion and higher electronic conductivity of the composite lead to higher ORR activity. The order of ORR activity is the optimized result of Pt on above two factors. The OER activity is mainly determined by Ir and IrO_2, and their ratio in the composite, for Pt (with some OER activity) was kept constant in each catalyst. Individual IrO_2 has a little higher OER activity than individual Ir. Moreover, OER activity of IrO_2 can be further enhanced by depositing appropriate Ir on IrO_2 surface to improve the conductivity (IrO_2 surface modification). Too lower Ir content leads to incomplete IrO_2 surface modification, and too higher Ir content leads to lower IrO_2 content (keeping the total constant), thereby lower OER activity. Therefore, the order of OER activity is the result of IrO_2 surface modification, which is different from the order of ORR activity.

3.5. ORR kinetic analysis of $Pt/Ir_3(IrO_2)_7$ catalyst

As is known, ORR on Pt catalyst is a rather complex process involved 2-electron mechanism or 4-electron mechanism which determines the ORR efficiency, and it is the key issue to fabricate 4-electron-mechanism oriented electrocatalyst. Fig. 6a shows polarization curves for ORR on $Pt/Ir_3(IrO_2)_7$ catalyst measured

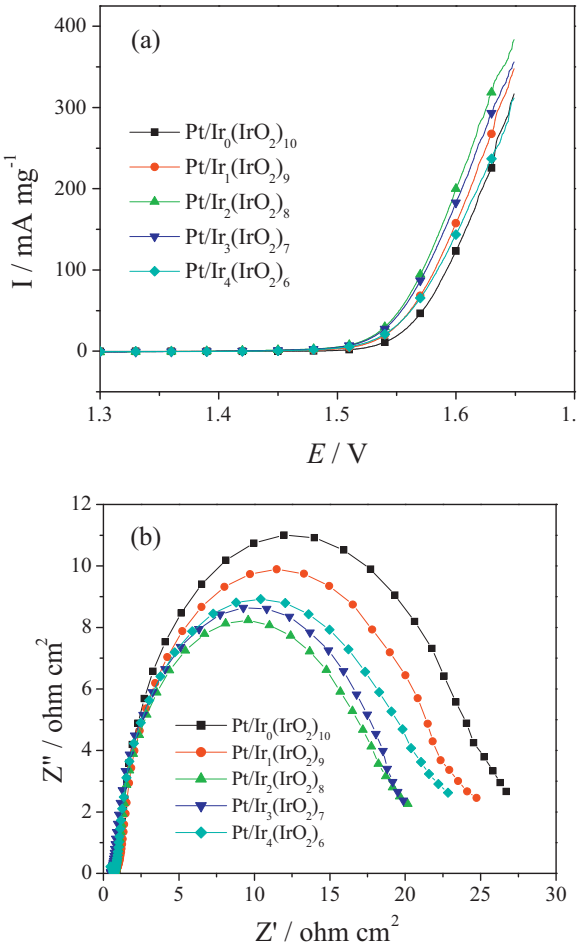

Fig. 5. Oxygen evolution activity measured with LSV (a), and EIS (1.50 V) (b) as a function of various compositions of $Pt/Ir_x(IrO_2)_{10-x}$ catalysts.

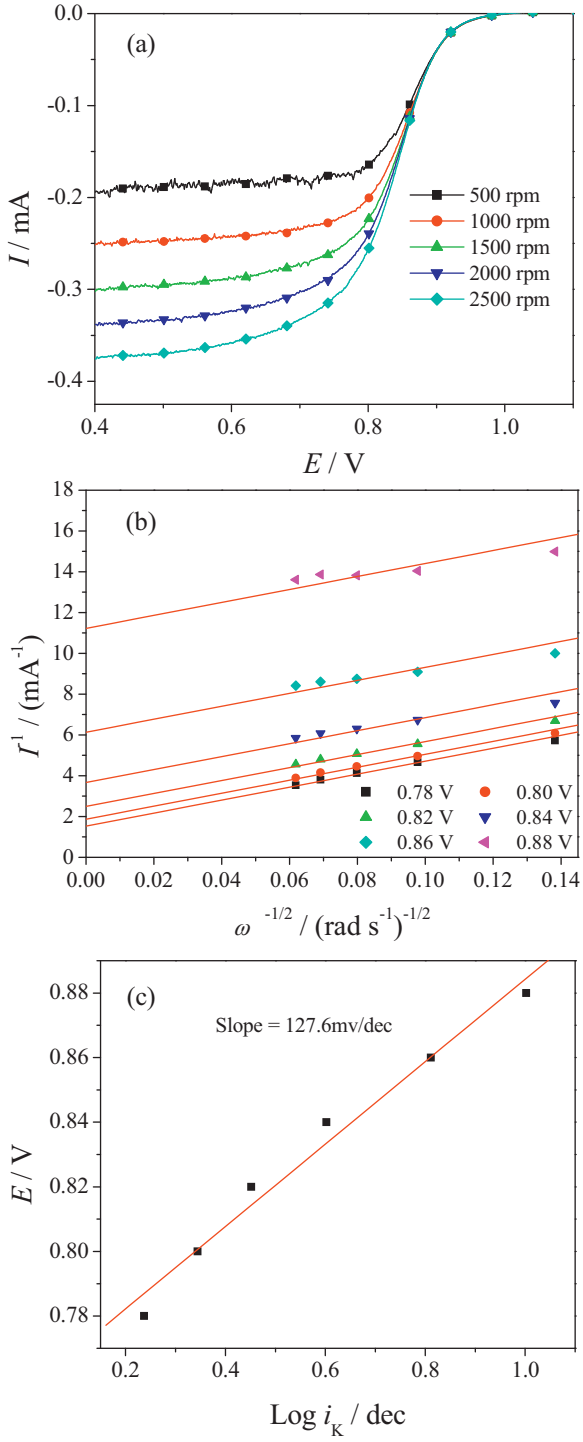

Fig. 6. ORR polarization curves at different rotation speeds (a), Koutecky–Levich plots at 0.80, 0.75, 0.7, 0.65 V (b), and $E - \log I_k$ curve (c) on $Pt/Ir_3(IrO_2)_7$.

at different rotation speeds at 5 mV s^{-1}. Well-defined limiting currents are observed as a function of rotation speeds in the diffusion-control region. The relationship between oxygen reduction current and rotation speed at a thin catalyst layer on GC RDE is given by Koutecky–Levich equation [35,36],

$$\frac{1}{I} = \frac{1}{I_k} + \frac{1}{B\omega^{1/2}} \quad (2)$$

where I is the experimentally obtained current, I_k is the kinetic current, B is the Levich slope and ω is the rotation speed of RDE. The Levich slope is given by,

$$B = 0.62nFAD^{2/3}\nu^{-1/6}c \quad (3)$$

where n is the number of electrons transferred per oxygen molecule, F is the Faraday constant, A is the surface area of the electrode, D is the diffusion coefficient of oxygen in the solution, ν is the kinetic viscosity of the solution, and c is the concentration of oxygen in the solution.

Fig. 6b shows I^{-1} vs. $\omega^{-1/2}$ plots for oxygen reduction measured at 0.80, 0.75, 0.7, and 0.65 V. A linear relationship between I^{-1} and $\omega^{-1/2}$ is observed and the approximately identical slopes indicate that oxygen reduction reaction on $Pt/Ir_3(IrO_2)_7$ catalyst follows the first order kinetics. In addition, the slope of the straight line, so-called 'B-factor', allows the number of electrons involved in the ORR to be estimated. Based on Eqs. (1) and (2), calculation for n was performed using the B value (0.0314) obtained through the slope of the straight line in Fig. 6b, and the literature data [35,37]: F, 96,485 C mol^{-1}; A, 0.07065 cm^2; D, 1.93×10^{-5} cm^2 s^{-1}; ν, 9.87×10^{-3} cm^2 s^{-1}; c, 1.18×10^{-6} mol cm^{-3}. The resultant n value is approximately 4, which is in good agreement with four-electron reaction mechanism. Fig. 6c presents the Tafel plot of $Pt/Ir_3(IrO_2)_7$ catalyst for ORR. It reveals the relationship between potential, E, and kinetic current, I_k. I_k is obtained by the straight-line intercept on I^{-1} axis in Fig. 6b. The Tafel slope of the straight line is estimated to be 127.6 mV dec^{-1}, which is quite close to that of pure Pt (120 mV dec^{-1}).

4. Conclusions

In the present study, bifunctional oxygen electrocatalyst, $Pt/Ir_x(IrO_2)_{10-x}$, has been prepared by depositing Pt on $Ir_x(IrO_2)_{10-x}$ support. Uniformly distributed $Pt/Ir_x(IrO_2)_{10-x}$ nanocomposites are obtained. $Pt/Ir_3(IrO_2)_7$ catalyst possesses the highest electrochemical active area and the highest activity towards oxygen reduction reaction among the series of catalysts studied. And it also exhibits excellent activity towards oxygen evolution reaction. The enhanced performance of $Pt/Ir_3(IrO_2)_7$ catalyst can be attributed to the introduction of Ir into IrO_2 support, which improves electronic conductivity and the overall performance.

Acknowledgements

This work is financially supported by National Natural Science Foundation of China (Grant No. 50872027, 21106024, and 21173062), Ministry of Science and Technology of China (863 program Grant No. 2009AA05Z111), Fundamental Research Funds for the Central Universities (HIT.ICRST.2010006), and Natural Scientific Research Innovation Foundation in Harbin Institute of Technology (XWQQ5750012411).

References

[1] L.L. Swette, A.B. Laconti, S.A. McCatty, J. Power Sources 47 (1994) 343–351.
[2] S.D. Song, H.M. Zhang, P. Xiao, Z.G. Shao, T.B. Richar d, B.L. Yi, Int. J. Hydrogen Energy 33 (2008) 4955–4961.
[3] S.-D. Yim, W.-Y. Lee, Y.-G. Yoon, Y.-J. Sohn, G.-G. Park, T.-H. Yang, C.-S. Kim, Electrochim. Acta 50 (2004) 713–718.
[4] F. Barbir, T. Molter, L. Dalton, Int. J. Hydrogen Energy 30 (2005) 351–357.
[5] Z.G. Shao, B.L. Yi, M. Han, J. Power Sources 79 (1999) 82–85.
[6] J. Maclay, J. Brouwer, G. Samuelsen, Int. J. Hydrogen Energy 31 (2006) 994–1009.
[7] H.Y. Lee, J.Y. Kim, J.H. Park, Y.G. Joe, T.H. Lee, J. Power Sources 131 (2004) 188–193.
[8] J. Pettersson, B. Ramsey, D. Harrison, J. Power Sources 157 (2006) 28–34.
[9] H.P. Dhar, J. Appl. Electrochem. 23 (1993) 32–37.
[10] F. Mitlitsky, B. Myers, A.H. Weisberg, Energy Fuels 12 (1998) 56–71.
[11] L. Jörissen, J. Power Sources 155 (2006) 23–32.
[12] H.Y. Jung, S. Park, B.N. Popov, J. Power Sources 191 (2009) 357–361.
[13] S.D. Yim, G.G. Park, Y.J. Sohn, W.Y. Lee, Y.G. Yoon, T.H. Yang, S.k. Um, S.P. Yu, C.S. Kim, Int. J. Hydrogen Energy 30 (2005) 1345–1350.
[14] G. Chen, D.A. Delafuente, S. Sarangapani, T.E. Mallouk, Catal. Today 67 (2001) 341–355.
[15] T. Ioroi, N. Kitazawa, K. Yasuda, Y. Yamamoto, H. Takenaka, J. Electrochem. Soc. 147 (2000) 2018–2022.
[16] Z.D. Wei, S.G. Chen, Y. Liu, C.X. Sun, Z.G. Shao, P.K. Shen, J. Phys. Chem. C 111 (2007) 15456–15463.
[17] S. Zhang, Y.Y. Shao, X.H. Li, Z.M. Nie, Y. Wang, J. Liu, G.P. Yin, Y.H. Lin, J. Power Sources 195 (2010) 457–460.
[18] S.H. Sun, G.X. Zhang, D.S. Geng, Y.G. Chen, R.Y. Li, M. Cai, X.L. Sun, Angew. Chem. Int. Ed. 50 (2011) 422–426.
[19] S. Zhang, Y. Shao, G. Yin, Y. Lin, Appl. Catal. B: Environ. 102 (2011) 372–377.
[20] S. Fierro, A. Kapalka, C. Comninellis, Electrochem. Commun. 12 (2010) 172–174.
[21] S. Siracusano, V. Baglio, C. D'Urso, V. Antonucci, A.S. Aricò, Electrochim. Acta 54 (2009) 6292–6299.
[22] L. Ouattara, S. Fierro, O. Frey, M. Koudelka, C. Comninellis, J. Appl. Electrochem. 39 (2009) 1361–1367.
[23] Y.J. Zhang, C. Wang, N.F. Wan, Z.Q. Mao, Int. J. Hydrogen Energy 32 (2007) 400–404.
[24] W.L. Yao, J. Yang, J.L. Wang, Y. Nuli, Electrochem. Commun. 9 (2007) 1029–1034.
[25] U. Wittstadt, E. Wagner, T. Jungmann, J. Power Sources 145 (2005) 555–562.
[26] R. Adams, R.L. Shriner, J. Am. Chem. Soc. 45 (1923) 2171.
[27] J. Cheng, H. Zhang, H. Ma, H. Zhong, Y. Zou, Int. J. Hydrogen Energy 34 (2009) 6609–6613.
[28] Z.Z. Jiang, Z.B. Wang, D.M. Gu, E.S. Smotkin, Chem. Commun. 46 (2010) 6998–7000.
[29] S. Zhang, Y. Shao, H. Liao, M.H. Engelhard, G. Yin, Y. Lin, ACS Nano 5 (2011) 1785–1791.
[30] Y.Y. Shao, S. Zhang, C.M. Wang, Z.M. Nie, J. Liu, Y. Wang, Y.H. Lin, J. Power Sources 195 (2010) 4600–4605.
[31] J.J. Wang, G.P. Yin, H. Liu, R.Y. Li, R.L. Flemming, X.L. Sun, J. Power Sources 194 (2009) 668–673.
[32] S. Zhang, Y.Y. Shao, G.P. Yin, Y.H. Lin, Angew. Chem. Int. Ed. 49 (2010) 2211–2214.
[33] W.L. Xu, X.C. Zhou, C.P. Liu, W. Xing, T.H. Lu, Electrochem. Commun. 9 (2007) 1002–1006.
[34] S. Zhang, Y.Y. Shao, G.P. Yin, Y.H. Lin, J. Mater. Chem. 20 (2010) 2826–2830.
[35] J. Maruyama, I. Abe, J. Electroanal. Chem. 545 (2003) 109–115.
[36] S. Zhang, Y.Y. Shao, G.P. Yin, Y.H. Lin, J. Mater. Chem. 19 (2009) 7995–8001.
[37] V. Stamenkovic, T.J. Schmidt, P.N. Ross, N.M. Markovic, J. Electroanal. Chem. 554–555 (2003) 191–199.